The Journal of Chemical Physics

RESEARCH ARTICLE | AUGUST 08 2023

# Growth rate of $CO_2$ and $CH_4$ hydrates by means of molecular dynamics simulations

S. Blazquez ; M. M. Conde ; C. Vega ; E. Sanz



*J. Chem. Phys.* 159, 064503 (2023)
https://doi.org/10.1063/5.0160517

The Journal of Chemical Physics ARTICLE pubs.aip.org/aip/jcp

# Growth rate of $CO_2$ and $CH_4$ hydrates by means of molecular dynamics simulations

Cite as: J. Chem. Phys. 159, 064503 (2023); doi: 10.1063/5.0160517
Submitted: 2 June 2023 • Accepted: 24 July 2023 •
Published Online: 8 August 2023



S. Blazquez,[1] M. M. Conde,[2] C. Vega,[1] and E. Sanz[1,a)]

## AFFILIATIONS

[1] Departamento de Química Física, Facultad de Ciencias Químicas, Universidad Complutense de Madrid, 28040 Madrid, Spain
[2] Departamento de Ingeniería Química Industrial y del Medio Ambiente, Escuela Técnica Superior de Ingenieros Industriales, Universidad Politécnica de Madrid, 28006 Madrid, Spain

**Note:** This paper is part of the JCP Special Topic on Porous Solids for Energy Applications.
[a)]**Author to whom correspondence should be addressed:** esa01@ucm.es

## ABSTRACT

$CO_2$ and $CH_4$ hydrates are of great importance both from an energetic and from an environmental point of view. It is therefore highly relevant to quantify and understand the rate with which they grow. We use molecular dynamics simulations to shed light on the growth rate of these hydrates. We put the solid hydrate phase in contact with a guest aqueous solution in equilibrium with the pure guest phase and study the growth of both hydrates at 400 bars with temperature. We compare our results with previous calculations of the ice growth rate. We find a growth rate maximum as a function of the supercooling in all cases. The incorporation of guest molecules into the solid structure strongly decelerates hydrate growth. Consistently, ice grows faster than either hydrate and the $CO_2$ hydrate grows faster than the $CH_4$ one because of the higher solubility of $CO_2$. We also quantify the molecular motion required to build the solids under study and find that the distance traveled by liquid molecules exceeds by orders of magnitude that advanced by any solid. Less molecular motion is needed in order for ice to grow as compared to the hydrates. Moreover, when temperature increases, more motion is needed for solid growth. Finally, we find a good agreement between our growth rate calculations and experiments of hydrate growth along the guest–solution interface. However, more work is needed to reconcile experiments of hydrate growth toward the solution among each other and with simulations.





## I. INTRODUCTION

Clathrate hydrates, also known as gas hydrates, are a type of inclusion compound in which water molecules form a cage-like structure to trap small molecules.[1–5] They are commonly found in permafrost regions, continental margins, and deep sea sediments, where they can store large amounts of methane and other hydrocarbon gases.[6–8] Clathrate hydrates have gained significant attention in recent years due to their potential as an unconventional source of energy[1,8–15] and their role in global climate change.[16–18]

For example, methane hydrates represent a potentially vast source of natural gas.[1,8,9,15] In addition, the release of methane from hydrates due to warming temperatures has been identified as a significant contributor to global warming, as methane is a potent greenhouse gas.[19] On the other hand, $CO_2$ hydrates have potential applications in gas storage and transportation[17,20,21] and are also of interest for their role in mitigating climate change.[22]

Therefore, there is a growing need to understand the formation, stability, and behavior of clathrate hydrates, both for their potential as an energy source and their impact on the environment.

The formation of a hydrate from its molecular constituents can be divided in two distinct steps:[23] *nucleation* of a crystal embryo followed by its subsequent *growth*. Both experiments[23–31] and molecular simulations have been used to characterize each of these steps.[16,32–43]

In this paper, we use molecular dynamics simulations to estimate the growth rate of both methane and carbon dioxide hydrates. We employ the TIP4P/Ice water model, which has proved successful in predicting ice growth rates[44,45] and three phase equilibrium temperature ($T_3$) of hydrates.[46,47] We compare our simulation results with experimental measurements and obtain a satisfactory agreement.[24–26,48] Our results are at odds, however, with previous calculations of the growth rate using a different force field.[49]

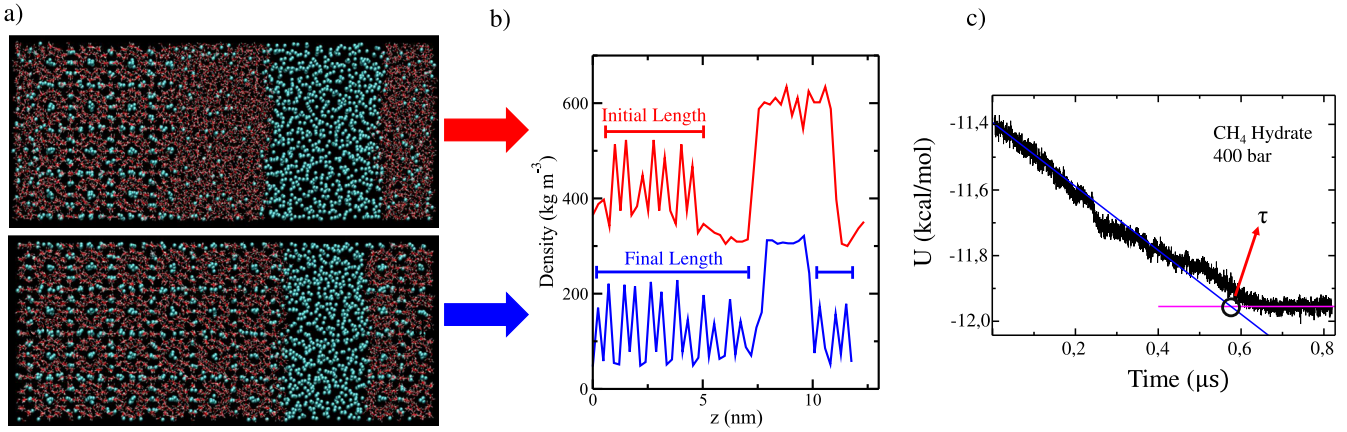


**FIG. 1.** (a), top: Initial configuration of a slab of methane hydrate put in contact with an aqueous solution of methane which is also in contact with gas methane at 400 bars and 280 K. (a), bottom: Final configuration after the hydrate has completely grown at 400 bars and 280 K incorporating all water molecules from the solution alongside the required methane molecules. In both snapshots, water molecules are represented as sticks in red and white colors, and methane molecules are represented as cyan spheres. (b) Density profile of $CH_4$ along the direction perpendicular to the interfaces. In red, the profile for the initial configuration (after 5 ns of equilibration). In blue, the profile for the final configuration. The profile of the initial configuration has been shifted 300 kg m$^{-3}$ upward to enable a clearer visualization of the comparison between both density profiles. The horizontal segments indicate the length of the hydrate phase in each case. (c) Potential energy per mole of molecules as a function of time along the simulation of methane hydrate growth, in black. The blue straight line corresponds to a fit to the first part of the growth whereas the pink horizontal line indicates the average potential energy reached when growth is completed. The intersection between both lines gives the growth time, $\tau$.

Overall, we propose a reliable simulation setup to estimate a parameter as important in the formation of hydrates as the growth rate.

## II. SIMULATION DETAILS

The TIP4P/Ice potential[50] is used to model water. This model includes one Lennard-Jones (LJ) site and three point charges. Methane is modeled using a LJ interaction site, and the parameters are provided in Refs. 51 and 52. $CO_2$ is modeled with three LJ sites whose parameters are given by the TraPPe potential.[53] The LJ parameters for the water–methane interaction were obtained using the default Lorentz–Berthelot rules. As for the $CO_2$–water LJ interactions, the distance parameter was obtained via the standard Lorentz–Berthelot rule, while the energy parameter was obtained by multiplying by 1.13 the value obtained using the default Lorentz–Berthelot rule following Ref. 47.

All simulations are performed using the molecular dynamics GROMACS package (version 4.6.5)[54,55] in the *NpT* ensemble and at a fixed pressure of 400 bars. We use the leap-frog integrator algorithm[56] with a time step of 2 fs. The temperature is fixed using the Nosé–Hoover thermostat[57,58] with a coupling constant of 2 ps. We have employed an anisotropic Parrinello–Rahman barostat[59] along the three axes with a relaxation time of 2 ps. This allows independent fluctuations and changes in the shape of the solid region to avoid stress in the solid. The cutoff radius employed for van der Waals and electrostatic interactions is 0.9 nm. We also applied long-range energy and pressure corrections to the LJ part of the potential. The smooth Particle Mesh Ewald (PME) method[60] is used to account for the long-range electrostatic forces. The geometry of the water molecules is maintained by applying the Linear Constraint Solver (LINCS) algorithm.[61,62]

## III. METHODOLOGY

### A. Determination of the growth rate

The procedure used to calculate hydrate growth rates in this study is summarized in Fig. 1. In Fig. 1(a), top, we present a snapshot of a typical simulation setup, where a slab of hydrate is put in contact with an aqueous solution of the guest molecule. The solution, in turn, is in contact with a guest reservoir. When the simulation is carried out below the temperature $T_3$ (the temperature at which all three phases—fluid guest, hydrate, and aqueous solution—are in equilibrium), the hydrate grows at the expense of the solution until all water molecules are integrated into the hydrate, as seen in the snapshot of Fig. 1(a) at the bottom. All the studied systems in this work (except one used for a specific case to analyze finite-size effects) consist of 2944 water molecules and 512 methane (or carbon dioxide) molecules in the hydrate structure (i.e., a $4 \times 4 \times 4$ unit cell), 3000 water molecules in the liquid slab, and 1000 $CH_4$ or $CO_2$ molecules in the guest phase. Some of these 1000 guest molecules are dissolved in the aqueous phase until guest–solution equilibrium is reached. Notice that when all water molecules are incorporated into the hydrate, around half of the molecules of the guest still remain in the reservoir.

In Fig. 1(b), we show the corresponding guest molecule density profiles for the configurations displayed in part a. The sharp peaks in the density profiles correspond to the hydrate region, whose length is indicated by a segment in Fig. 1(b). Each segment starts and ends at half the height of the first and the last solid peaks, respectively. By subtracting the initial hydrate length from the final one, we obtain the length grown by the hydrate, denoted as $\Delta L$.

To estimate the time required for hydrate growth, denoted as $\tau$, we use plots of the potential energy vs time, as shown in Fig. 1(c). As the hydrate grows, the potential energy decreases until all available water molecules (along with the required guest molecules) are

**TABLE I.** Growth rate of $CO_2$ and $CH_4$ hydrates at 400 bars and different temperatures using the TIP4P/Ice model. The numbers in parenthesis represent the uncertainty of the results.

| | $CO_2$ | | $CH_4$ | |
|---|---|---|---|---|
| T (K) | ΔT (K) | $u$(cm/s) | ΔT (K) | $u$(cm/s) |
| 280 | 11 | 2.62(20) | 14 | 0.36(3) |
| 270 | 21 | 2.94(20) | 24 | 0.42(4) |
| 270[a] | 21 | 3.04(20) | | |
| 260 | 31 | 2.89(30) | 34 | 0.49(3) |
| 250 | 41 | 1.79(10) | 44 | 0.33(2) |
| 240 | 51 | 1.15(10) | 54 | 0.26(2) |

[a]Result of the $CO_2$ hydrate computed with a system having an aqueous phase approximately twice as long as that of the rest of studied systems.

consumed and the potential reaches a plateau. The time required to reach such plateau is an estimate for $\tau$. In the final stage of growth, the solution structure can be affected by the proximity of the gas-solution interface. Moreover, one hydrate front typically arrives earlier than the other to the reservoir interface because the solution length at both sides of the hydrate slab is not the same. To exclude growth in such conditions and focus only on the growth along bulk-like solution, we fit the initial part of the potential energy plot (for time less than ~300 ns) to a straight line [blue line in Fig. 1(c)] and extrapolate this trend to the average potential energy value reached at the end of the simulation when the hydrate is completely grown [pink line in Fig. 1(c)]. The intersection between these two straight lines provides $\tau$. The growth rate, denoted as $u$, is simply obtained by dividing the length of the grown hydrate, $\Delta L$, by $2\tau$ due to the fact that there are two interfaces growing under periodic boundary conditions.

Five independent estimates of the growth rate are averaged for each temperature to obtain the growth rates reported in Table I. The variability between different simulations is illustrated in Fig. 2 where we plot the potential energy time evolution of five different trajectories of the growth of a $CO_2$ hydrate at 400 bars and 250 K. As can be seen, although the slope of the initial part of the growth (first ~250 ns) shows some stochasticity, it does not significantly change from one trajectory to another. Note also that the variability in growth rate is reflected in the error bars reported in Table I. Our estimate of growth rates for both hydrates has a relative error of about 10%.

## IV. RESULTS

### A. Hydrates vs ice growth rate

The growth rates determined as explained in Sec. III are plotted as a function of temperature in Fig. 3(a), where we compare the results for $CO_2$ and $CH_4$ hydrates obtained in this work (black and blue symbols, respectively) with the ice Ih growth rate (red curve) interpolated at 400 bars from previous studies[44,45,63] as explained in the Appendix of this work.

We first note that the growth rate of the solids under comparison is of the order of cm/s. This is consistent with the experimental observation of ice and hydrate growth in the order of seconds/minutes.[24,25,48,64,65] For a given temperature, ice Ih grows

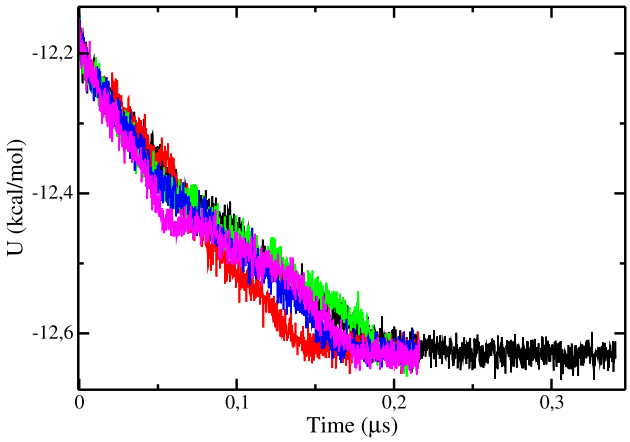


**FIG. 2.** Potential energy per mole of molecules as a function of time for five different growth trajectories of a $CO_2$ hydrate at 400 bars and 250 K. Different trajectories are started by assigning different Maxwellian velocities to the same initial configuration.

faster than either hydrate. This is unsurprising given that ice is only composed of water molecules whereas hydrates require both water and a guest molecule to build up their structure. The $CO_2$ hydrate grows faster than the $CH_4$ hydrate. This is also an expected behavior given the higher solubility of $CO_2$ as compared to that of $CH_4$. At 400 bars, and in the 240–280 K temperature range studied in this work, an aqueous solution in equilibrium with liquid $CO_2$ contains ~5–10 $CO_2$ molecules per 100 water molecules,[66] whereas a $CH_4$ aqueous solution in contact with methane gas contains approximately ten times less $CH_4$ molecules per 100 water molecules.[67] $CO_2$ being almost ten times more soluble than $CH_4$, it is then not surprising that carbon dioxide hydrates grow faster because they have more guest molecules available in the solution from which they grow. Bear in mind that the concentration of guest molecules in the solid hydrate is much larger than that in the solution (there are 17.4 guest molecules every 100 water molecules for fully occupied hydrates), so the incorporation of guest molecules into the growing solid is necessarily a limiting factor for the growth. That the solubility of $CO_2$ is larger than that of $CH_4$ can be understood by realizing that $CO_2$ is a liquid whereas $CH_4$ is a gas in the thermodynamic conditions under study.

Therefore, the concentration of guest molecules in the aqueous solution is key to hydrate growth and deserves careful inspection. In our simulation setup [see Fig. 1(a)], the solution is in contact on one side with the growing hydrate and on the other with the guest reservoir. We find that as the hydrate grows, the concentration of guest molecules in the middle of the solution reaches a steady value. The guest concentration will be set by the reservoir–solution equilibrium if the hydrate grows slowly, whereas it will be depleted by the hydrate if it grows fast. To elucidate which of these situations actually takes place, we compare the steady state concentration in the middle of the solution obtained during our growth simulations with the solution–reservoir equilibrium concentration reported in previous studies.[66,67] The comparison is established in Fig. 4. Whereas the concentration of methane is clearly given by the equilibrium value, that of $CO_2$ is depleted by the quick incorporation of $CO_2$ molecules into the growing hydrate. Seemingly, the growth of the methane

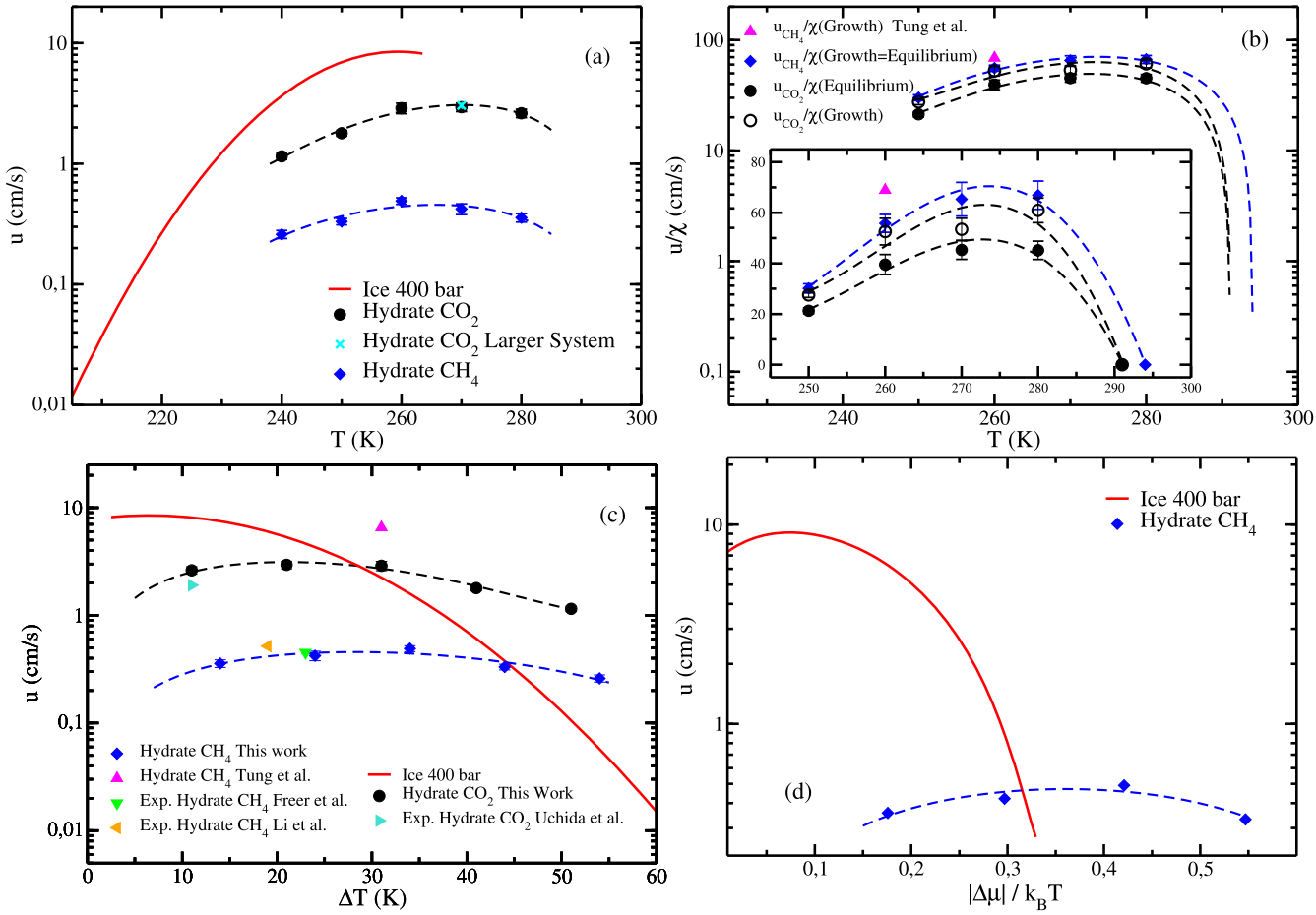


**FIG. 3.** (a) Growth rate at 400 bars as a function of temperature. The red curve corresponds to the growth of ice along the direction perpendicular to the secondary prismatic direction and it is taken from Refs. 44 and 45 and interpolated as explained in the Appendix. Black circles and blue diamonds correspond to the growth of $CO_2$ and $CH_4$ hydrates, respectively (this work). The cyan cross is the growth rate of the $CO_2$ hydrate computed with a system having an aqueous phase approximately twice as long as that of the rest of the studied systems. Dashed lines are cubic fits for visual guidance. (b) Growth rate divided by the guest molecule molar fraction in the aqueous solution as a function of temperature. For $CO_2$, two different molar fractions are considered: the solution–reservoir equilibrium concentration (filled black circles) and the steady $CO_2$ concentration in the middle of the solution during growth (open black circles). For $CH_4$, both concentrations coincide (see Fig. 4) and there is a single curve (blue diamonds). The solution–reservoir equilibrium solubilities have been taken from Ref. 67 for $CH_4$ and from Ref. 66 for $CO_2$. The pink up-triangle corresponds to $CH_4$ hydrate simulation data taken from Ref. 49 rescaled by the concentration during growth. The inset shows the same plot as the main figure but with the y-axis in a linear instead of a logarithmic scale. (c) Growth rates as a function of supercooling condition. We compare our results with experimental data for the growth rate of $CO_2$ hydrates taken from the work of Uchida *et al.*[25] (cyan right triangle), with simulation results for the growth rate of the $CH_4$ hydrate presented in the study of Tung *et al.*[49] (pink up triangle) and with experiments of $CH_4$ hydrate growth presented in the study of Freer *et al.*[24] (green down triangle) and Li *et al.*[48] (orange left triangle) (extrapolated to our pressure of interest as explained in the Appendix). (d) Growth rates of ice and $CH_4$ hydrate as a function of chemical potential difference per water particle between the solid and the liquid.

hydrate is slow enough to enable a steady equilibrium-like concentration, whereas that of the $CO_2$ hydrate is too fast. Such a kinetic effect on the $CO_2$ concentration could be dependent on the distance between the hydrate front and the solution–reservoir interface. To quantify this possible system-size dependence, we have recomputed the concentration and the $CO_2$ hydrate growth rate with a system having approximately a solution twice as long. This has been done for a specific temperature (270 K) and a system consisting of the same number of molecules in the hydrate phase but increasing the number of liquid water molecules (6660) and the number of liquid $CO_2$ molecules (3000). The result of this calculation is shown with a cyan cross in Figs. 3(a) and 4. Our data show that neither the concentration in the middle of the solution nor the growth rate depends on the length of the aqueous phase. Perhaps, a more systematic study is required in the future to establish a relationship between growth rate and simulation box length in $CO_2$ hydrates.

To further quantify the effect of guest molecule solubility on growth velocity, we compare in Fig. 3(b) the growth rates of both hydrates divided by the corresponding guest molar fraction in the aqueous solution. In the case of $CO_2$, we obtain two curves: one dividing by the solution–reservoir equilibrium concentration[66] and another by the steady concentration obtained during our growth simulations (for methane, both concentrations coincide as discussed in the previous paragraphs, so there is a single curve). Regardless

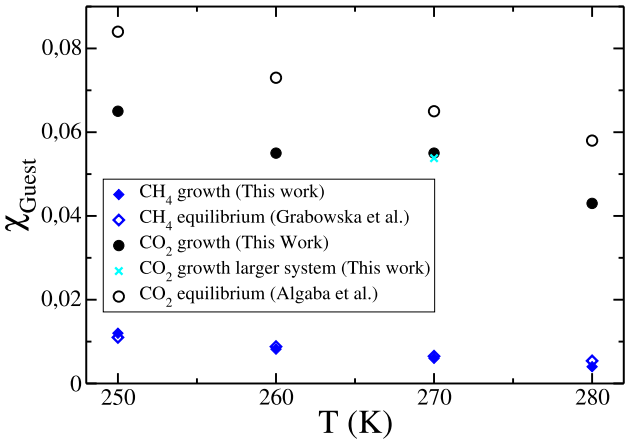


**FIG. 4.** Steady guest concentration (in molar fraction) in the middle of the solution during hydrate growth (filled black circles for $CO_2$ and filled blue diamonds for $CH_4$) compared to the solution–reservoir equilibrium concentration reported in the study of Algaba *et al.*[66] for $CO_2$ (empty black circles) and the study of Grabowska *et al.*[67] for $CH_4$ (empty blue diamonds) for the temperatures studied in this work. The cyan cross is the $CO_2$ concentration during growth obtained with a larger system (see main text).

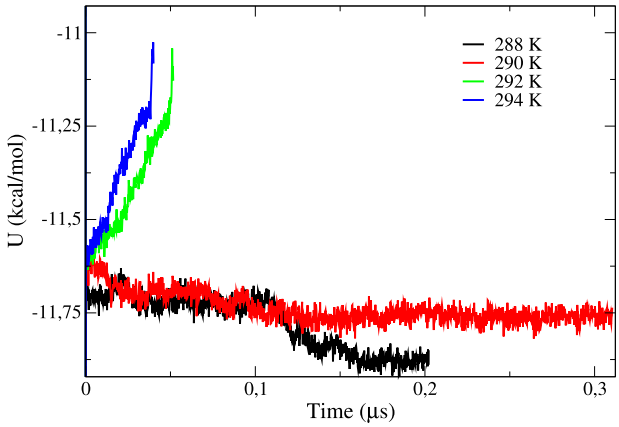


**FIG. 5.** Time evolution for different temperatures (as indicated in the legend) and at 400 bars of the potential energy of a $CO_2$ hydrate per mole of particles (which means that we have divided the energy by the total number of particles of the system and multiplied by the Avogadro number) in contact with a $CO_2$ aqueous solution in equilibrium with liquid $CO_2$ [the initial configuration is similar to that shown in Fig. 1(a), top, but with $CO_2$ instead of methane].

of the concentration used for the rescaling, the difference between the concentration-scaled growth rates is much smaller than before the scaling. The $CO_2$ curve rescaled by the concentration during growth is closer to the $CH_4$ curve than that rescaled by the equilibrium concentration, suggesting that the relevant concentration is the actual concentration near the hydrate front. Curiously, the $CH_4$ hydrate concentration-scaled growth rate seems to be systematically larger than that of the $CO_2$ hydrate. This would suggest that, for a given concentration, molecules with symmetry close to spherical, like methane, lead to a faster hydrate growth as compared to nonspherical molecules like $CO_2$. However, the $CH_4$ and the $CO_2$ datasets lie within error bars when the $CO_2$ hydrate growth rate is scaled by the concentration during growth, so this conclusion about the influence of molecular shape on growth speed has to be interpreted/treated with caution.

In Fig. 3(c), we plot the growth rate as a function of supercooling, $\Delta T$, which is the difference between the temperature at which the solid melts and the temperature of interest. The melting point of ice Ih at 400 bars is 266 K as interpolated from previous work.[44,63,68] The dissociation temperature for the $CH_4$ hydrate at 400 bars obtained for the same system size and cutoff value used in this work is 294 K.[67] The dissociation temperature for the $CO_2$ hydrate has been calculated in this work by monitoring the potential energy of a three phase coexistence system[46,69,70] as that shown in Fig. 1(a), top (obviously, using $CO_2$ as a guest molecule). In Fig. 5, we show the time evolution of the potential energy of such system for different temperatures. At low temperatures, the potential energy goes down because the hydrate grows, whereas at high temperatures the potential energy goes up because the hydrate dissociates. Thus, we enclose the dissociation temperature of the $CO_2$ hydrate at 400 bars at 291 ± 2 K. The difference between this value and the 287 ± 2 K reported in Ref. 47 could be attributed both to the statistical error and to simulation details such as the cutoff or the employed system size.[71] Note that for a cutoff of 1.0 nm, we have very recently computed the $T_3$ using a different procedure based on the guest aqueous solubility in the solution–guest and solution–hydrate coexistences and we obtained a $T_3$ of 290(2) K, which is in good agreement with the result of this work.[66]

Knowing the melting/dissociation temperature of all solids under comparison, we can plot the growth rate as a function of supercooling, as shown in Fig. 3(c). When compared at the same $\Delta T$, the ice growth rate remains higher than that of the hydrates at low and moderate supercooling conditions but becomes smaller at high supercooling conditions. This can be understood by realizing that ice has a lower melting temperature than both hydrates.[72] Therefore, the same supercooling condition means a temperature about 25 K lower for ice. In fact, for the highest supercooling under comparison, the absolute temperature for the ice system is as low as 210 K, where diffusion is extremely slow (and so is ice growth).

Another interesting aspect is the presence of a maximum in the growth rate. Such a maximum occurs at a supercooling condition of 12 ± 5, 20 ± 10, and 30 ± 10 K for ice, $CO_2$ hydrate, and $CH_4$ hydrate, respectively. This growth rate temperature-dependence, which has been previously studied for ice,[44,45,73–75] can be understood as a result of two competing factors: (1) the thermodynamic driving force for the formation of the solid grows as temperature goes down; (2) the molecular diffusivity slows down on cooling.

In part (d) of Fig. 3, we plot the growth rates of both ice and the $CH_4$ hydrate as a function of $\Delta\mu/(k_BT)$, the chemical potential difference per water particle between the solid and the solution. We took $\Delta\mu/(k_BT)$ from Refs. 44 and 67 for ice and the methane hydrate, respectively. Regarding the case of methane hydrate, in Ref. 67 the chemical potentials of each component (methane and water) in each phase (hydrate and solution) as well as the stoichiometry of the hydrate were properly taken into account in the calculation of the chemical potential change due to the formation of

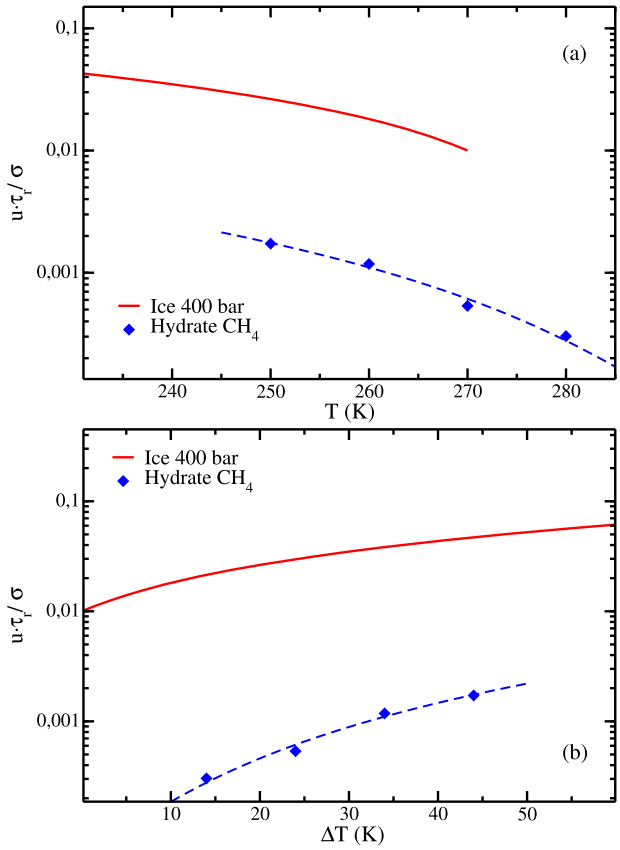


**FIG. 6.** Growth rate of ice and of the $CH_4$ hydrate at 400 bars multiplied by the time required to diffuse one molecular diameter ($\tau_r$) and divided by the molecular diameter of water ($\sigma$ = 3.1668 Å) as a function of (a) temperature and (b) supercooling. Results for the growth rate of ice are taken from Refs. 44 and 45 and interpolated as explained in the Appendix. The blue dashed line is a cubic fit to the $CH_4$ hydrate data.

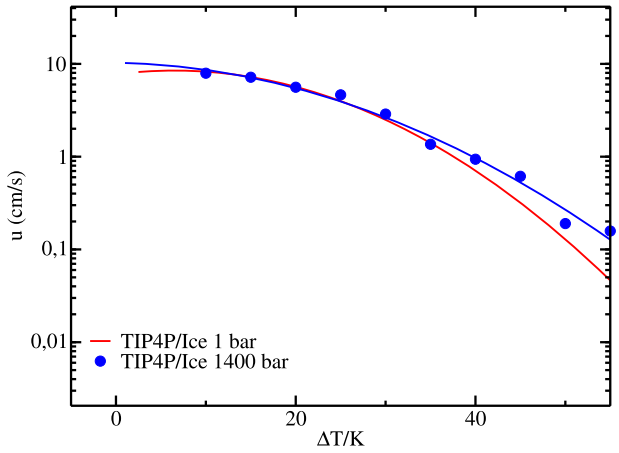


**FIG. 7.** Growth rate of ice (pII plane) vs supercooling for different pressures as indicated in the legend. The 1 and 1400 bars curves are taken from Refs. 44 and 63, respectively. In Ref. 63, these curves were plotted as a function of T instead of as a function of ΔT as in the present plot. This representation evidences the independence of $u$ with pressure for a constant ΔT.

the hydrate from the solution we use in this work [in Fig. 3(d) we simply report such chemical potential change per water molecule]. The chemical potential difference is the thermodynamic driving force for the formation of the solid. Since $\Delta\mu$ increases linearly with $\Delta T$,[44,67] $u(\Delta\mu)$ and $u(\Delta T)$ follow the same trend. The $u(\Delta\mu)$ data for ice lie well above those of the methane hydrate at low $\Delta\mu$ but fall below those of methane hydrate at high $\Delta\mu$ due, again, to the low temperature corresponding to the ice system at such high $\Delta\mu$.

It is interesting to express the growth rate of a solid in terms of molecular diameters per diffusive time instead of cm per second. In our case, we identify the molecular diameter, $\sigma$, with the LJ parameter of the water oxygen atom. The diffusive time, $\tau$, is the time at which the mean squared displacement of liquid water reaches a value of $\sigma^2$. Then, $\tau$ is approximately the time required for a water molecule to diffuse its own diameter. Obviously, $\tau$ increases as temperature decreases. The ratio between $u$ and $\sigma/\tau$, $u^* = u/(\sigma/\tau)$, gives information on the actual distance traveled by molecules in order to build up the solid. For instance, for $u^* = 1$ the solid grows 1 $\sigma$ as water molecules in the liquid diffuse their own diameter. In Figs. 6(a) and 6(b), we plot $u^*$ as a function of temperature and $\Delta T$, respectively, for ice and for the $CH_4$ hydrate as indicated in the legend. $u^*$ is much smaller than 1 for both solids, so water has to diffuse many times its own diameter in order for the solids to grow 1$\sigma$. In the case of ice, $u^*$ is close to 0.1 at low temperatures (high supercooling), so about ten molecular diameters are traveled by water liquid molecules to build 1$\sigma$ of solid. At high temperatures (low supercooling), $u^*$ drops to 0.01, so 1$\sigma$ of new solid requires water molecules diffusing about 100 times their own diameter. By comparing ice data to hydrate data, one realizes that, for a given temperature, $u^*$ is approximately one order of magnitude smaller for the methane hydrate. This means that water molecules need to diffuse about ten times more in order to build up the same amount of solid. Such a requirement for more molecular motion can be understood by taking into account that the hydrate has to concertedly arrange water and guest molecules in order to grow. It is also interesting to note that the variation of $u^*$ with $T$ has a negative slope. This means that the lower the temperature (the higher the supercooling), the more effective are molecular motions in building the solid. So, even though the solids grow slower at high supercooling conditions due to slow diffusion, the actual molecular displacements leading to solid growth are smaller.

## B. Comparison with other simulations

In Ref. 32, the growth mechanism of methane hydrates was investigated, but no quantitative predictions of the growth rate were reported. In Ref. 49, however, the authors of the work of Tung *et al.* reported growth rates for the methane hydrate. In Fig. 3(c), we show data from Ref. 49 as a pink upward triangle (to establish the comparison, we had to interpolate the data in Ref. 49 as described in the Appendix). The discrepancy between our data and that of Ref. 49 is extremely large—of more than one order of magnitude—and their predicted rate for the methane hydrate lies even above ours for

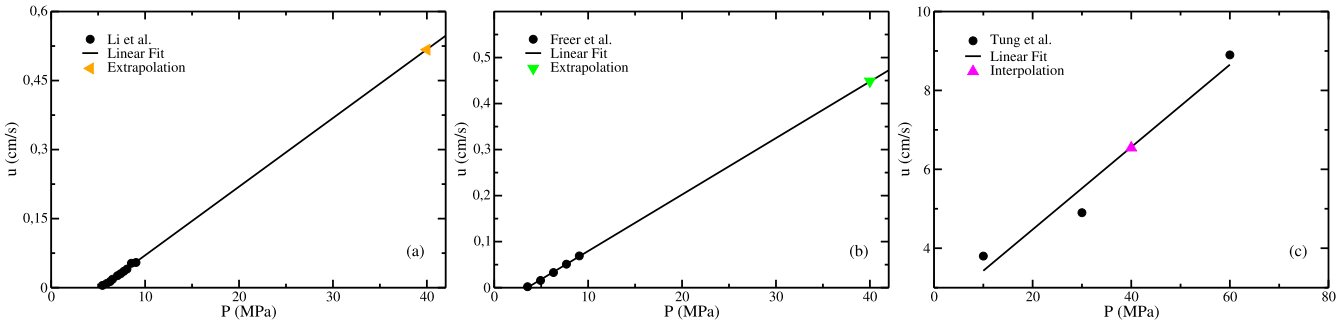


**FIG. 8.** Growth rates for methane hydrate vs pressure taken from literature data (black symbols) used to extrapolate/interpolate and obtain the data that we compare in Fig. 3(b) with our simulations (colored symbols). In (a), we show the extrapolation of the experimental data taken from Ref. 48 at T = 278 K, in (b) we show the extrapolation of the experimental data taken from Ref. 24 at T = 274 K and in (c) we show the interpolation of the simulation data given in Ref. 49 at T = 260 K.

the $CO_2$ hydrate. However, in Ref. 49 a different force field was employed to simulate methane hydrates. To understand the difference in predicted growth rates, we examine the solubility of methane in water predicted by each model. We focus on the solubility because we have seen in Fig. 3(b) that the growth rates of $CO_2$ and $CH_4$ hydrates become similar to each other when rescaled by the concentration of the corresponding guest molecule in the aqueous solution. At the temperature at which the comparison with the work of Tung *et al.*[49] is established, 260 K, the molar fraction of methane in the aqueous solution in equilibrium with methane gas is 0.0088 for our potential model. We get an approximate methane molar fraction of 0.095 for the force field employed in Ref. 49 by interpolating at pressure 400 bars the curves given in Fig. 8 of such publication. This value is approximately one order of magnitude larger than that predicted by our force field. To check if such a large difference in solubility can account for the discrepancy in the predicted growth rate, we compare in Fig. 3(b) the growth rates rescaled by the methane molar fraction. The difference between our data and that reported in the work of Tung *et al.* is now much smaller than that shown in Fig. 3(c), before the rescaling was made. This shows again that the solubility of the guest molecule plays a key role in the growth rate of the hydrate. The force fields employed in this work yield $CO_2$ and $CH_4$ solubilities of the same order as experimental ones at the pressure of interest.[47,67] This is perhaps a key issue in the successful comparison with experimental growth rates established in Sec. IV C.

### C. Comparison with experiments

Most experimental studies on hydrate growth[23–29] observe the propagation of the clathrate along the aqueous solution–guest interface. In Fig. 3(b), we compare our simulation results with three of these experimental papers. In order to establish the comparison, we had to extrapolate the experimental data as explained in detail in the Appendix. The agreement is strikingly satisfactory in all cases. This is quite surprising considering the fact that we are studying growth toward the aqueous phase rather than along the interface. A possible explanation is that the thickness of the hydrate layer that grows along the interface in the aforementioned experiments is large enough so as to make these experiments equivalent to our simulation setup.

Growth toward the aqueous phase was observed in Refs. 23 and 28, both dealing with $CO_2$ hydrates, and the scenario is a bit uncertain. In the work of Touil *et al.*,[23] crystalline fibers were reported to grow toward the bulk aqueous phase at $2 \times 10^{-2}$ cm/s at 10 bars and $-31\,^{\circ}C$ (29 degrees of supercooling). We cannot directly compare this measurement to our simulation values because the pressure is different. However, the observation in Ref. 23 seems inconsistent with the experiments performed in the work of Ou *et al.*,[28] where they observe slower growth rates even at higher pressure. For example, in conditions comparable to our simulations, 400 bars and 280.15 K, they observed growth of a hydrate front along a capillary at a rate of $2 \times 10^{-6}$ cm/s. These data are neither consistent with Ref. 23, which reports a much faster rate at a lower pressure, nor with our simulations (we predict growth rates about 6 orders of magnitude higher for methane hydrates in Fig. 3). Clearly, more work is needed to have simulation and experimental benchmark values of hydrate growth rates.

## V. SUMMARY AND CONCLUSIONS

We compute the growth rate of $CO_2$ and $CH_4$ hydrates with computer simulations using the TIP4P/Ice water model. We study different temperatures at 400 bars. Our simulations start with a hydrate slab in contact with an aqueous solution of the guest molecule in equilibrium with a slab of the pure guest phase. We run simulations below the three phase equilibrium temperature of the hydrate. Consequently, the hydrate grows at the expense of the solution. We estimate the growth rate through variation of the potential energy, which drops as the hydrate grows until a constant value is reached when all water molecules of the solution, alongside the corresponding guest molecules, are incorporated into the hydrate.

We compare the hydrates' growth rates obtained in this work with previous simulation results for the ice growth rate. For a given temperature, the growth rate of the hydrates is lower than that of ice by 1–2 orders of magnitude, which reflects that incorporating guest molecules into the solid lattice strongly slows down the growth. The slowing down effect of the guest on growth is further proven

by the fact that the $CH_4$ hydrate grows about one order of magnitude slower than the $CO_2$ hydrate, the $CH_4$ solubility being about one order of magnitude lower than that of $CO_2$. Moreover, when the growth rates are rescaled by the solubility of the corresponding guest molecule in the aqueous solution, the results for both hydrates become similar to each other.

We also compare growth rates for a given supercooling condition (difference between the melting temperature and the temperature of interest). We take the melting temperature of ice and of the $CH_4$ hydrate from the literature and compute that of the $CO_2$ hydrate. Ice grows faster than both hydrates at low supercooling conditions, although it grows slower at high supercooling conditions given that the absolute temperature is about 25 K smaller for the ice system for a given supercooling condition. This temperature difference is a consequence of the fact that the ice melting temperature is about 25 K lower than the dissociation temperature of the hydrates. The conclusion obtained when comparing growth rates for a constant chemical potential difference between the solid and the liquid is similar: For low chemical potential differences, ice grows faster, whereas for high differences ice grows slower than the hydrate.

We also analyze the ratio between molecular motion in the liquid and solid growth. Water diffuses many times its own diameter in the liquid as the solid grows only one molecular diameter for both ice and the $CH_4$ hydrate (we have not done this analysis for the $CO_2$ hydrate, although a similar conclusion is expected in this case). The diffusion required to build the hydrate is about ten times larger than that needed for ice to grow. As temperature goes down, less diffusion is needed to build the same amount of solid, even though the solid grows slower due to slower diffusion.

We compare our simulations with experimental data. Most experimental studies report hydrate growth along the interface between the solution and the guest phase. No direct measurements at 400 bars have been reported, so we had to extrapolate experimental data as explained in the Appendix. Good agreement is obtained between extrapolated measurements and our calculations. A couple of experimental papers report hydrate growth toward the solution and the results are not consistent with each other. The experiment performed at conditions comparable to our simulations is not in agreement with our predictions. Further work is needed to clarify this issue and to obtain benchmark values of hydrate growth rates.

## ACKNOWLEDGMENTS

This work was funded by Grant Nos. PID2019-105898GB-C21, PID2019-105898GA-C22, PID2022-136919NB-C31, and PID2022-136919NB-C32 of the MICINN. M.M.C. thanks CAM and UPM for financial support of this work through the CavItieS Project No. APOYO-JOVENES-01HQ1S-129-B5E4MM from "Accion financiada por la Comunidad de Madrid en el marco del Convenio Plurianual con la Universidad Politecnica de Madrid en la linea de actuacion estimulo a la investigacion de jovenes doctores" and CAM under the Multiannual Agreement with UPM in the line Excellence Program for University Professors, in the context of the V PRICIT (Regional Program of Research and Technological Innovation). The authors thank the Universidad Politecnica de Madrid (www.upm.es) for providing computing resources on the Magerit Supercomputer.

## AUTHOR DECLARATIONS

### Conflict of Interest

The authors have no conflicts to disclose.

### Author Contributions

**S. Blazquez**: Conceptualization (equal); Data curation (equal); Formal analysis (equal); Investigation (lead); Methodology (lead); Writing – original draft (lead); Writing – review & editing (equal). **M. M. Conde**: Conceptualization (equal); Funding acquisition (lead); Investigation (equal); Resources (lead); Supervision (equal); Writing – review & editing (equal). **C. Vega**: Conceptualization (equal); Data curation (equal); Formal analysis (equal); Funding acquisition (equal); Investigation (equal); Methodology (equal); Project administration (equal); Supervision (equal); Writing – original draft (equal); Writing – review & editing (equal). **E. Sanz**: Conceptualization (equal); Data curation (equal); Formal analysis (equal); Funding acquisition (lead); Investigation (equal); Project administration (lead); Supervision (equal); Writing – original draft (lead); Writing – review & editing (lead).

## DATA AVAILABILITY

The data that support the findings of this study are available within the article.

## APPENDIX: DETAILS ON THE COMPARISON WITH OTHER WORKS

The ice growth rate at 400 bars has been obtained from the results previously published for 1 and 1400 bars.[44,63] As seen in Fig. 7, the ice growth rate is almost pressure-independent for a given supercooling condition. Taking advantage of this property, we use the 1 bar u(ΔT) curve [given in Eq. (3) of Ref. 44] and then convert it to u(T) for 400 bars using the melting temperature corresponding to the latter pressure (266 K).[63]

The experimental data for $CO_2$ hydrates in Fig. 3(c) (right cyan triangle) have been obtained from Eq. (1) in the work of Uchida *et al.*,[25] where the growth rate is provided as a function of supercooling. According to such publication, the growth rate is pressure-independent, at least in the pressure range where the experiments were carried out: 18–72 bars. We therefore use the same expression for our pressure of interest.

Regarding methane hydrates, the experimental data from Refs. 24 and 48 were obtained by extrapolating a plot of the growth rate as a function of pressure at constant temperature as shown in Figs. 8(a) and 8(b). In the work of Li *et al.*,[48] the temperature was kept at 278 K, whereas in the work of Freer *et al.*[24] several temperatures were studied and we selected the data for 274 K. In both cases, the pressure dependency of the growth rate is linear in the studied pressure range (actually, the slope is consistent between both experimental datasets). Based on this linear behavior, we extrapolated to our pressure of interest (400 bars) both experimental rates. We acknowledge this is perhaps a wild extrapolation but we believe it is worth establishing a comparison nonetheless.

To compare our results with the simulation results reported in the work of Tung *et al.*,[49] we interpolated the growth rate vs pressure data reported in Ref. 49 as shown in Fig. 8(c).

## REFERENCES


[1]E. D. Sloan and C. A. Koh, *Clathrate Hydrates of Natural Gases*, 3rd ed. (CRC Press, 2007).
[2]J. A. Ripmeester, J. S. Tse, C. I. Ratcliffe, and B. M. Powell, "A new clathrate hydrate structure," Nature **325**, 135 (1987).
[3]R. K. McMullan and G. A. Jeffrey, "Polyhedral clathrate hydrates. IX. Structure of ethylene oxide hydrate," J. Chem. Phys. **42**, 2725–2732 (1965).
[4]T. C. W. Mak and R. K. McMullan, "Polyhedral clathrate hydrates. X. Structure of the double hydrate of tetrahydrofuran and hydrogen sulfide," J. Chem. Phys. **42**, 2732–2737 (1965).
[5]S. Alavi and J. A. Ripmeester, *Clathrate Hydrates: Molecular Science and Characterization* (John Wiley & Sons, 2022).
[6]C. Bourry, J. L. Charlou, J. P. Donval, M. Brunelli, C. Focsa, and B. Chazallon, "X-ray synchrotron diffraction study of natural gas hydrates from African margin," Geophys. Res. Lett. **34**, L22303, https://doi.org/10.1029/2007gl031285 (2007).
[7]H. Lu, Y. Seo, J. Lee, I. Moudrakovski, J. A. Ripmeester, N. R. Chapman, R. B. Coffin, G. Gardner, and J. Pohlman, "Complex gas hydrate from the Cascadia margin," Nature **445**, 303 (2007).
[8]E. Dendy Sloan, Jr., "Fundamental principles and applications of natural gas hydrates," Nature **426**, 353–359 (2003).
[9]R. Boswell, "Is gas hydrate energy within reach?," Science **325**, 957–958 (2009).
[10]H. Lee, J. Lee, D. Y. Kim, J. Park, Y. Seo, H. Zeng, I. L. Moudrakovski, C. I. Ratcliffe, and J. A. Ripmeester, "Tuning clathrate hydrates for hydrogen storage," Nature **434**, 743 (2005).
[11]A. Martin and C. J. Peters, "Hydrogen storage in sH clathrate hydrates: Thermodynamic model," J. Phys. Chem. B **113**, 7558 (2009).
[12]L. J. Florusse, C. J. Peters, J. Schoonman, K. C. Hester, C. A. Koh, S. F. Dec, K. N. Marsh, and E. Dendy Sloan, "Stable low-pressure hydrogen clusters stored in a binary clathrate hydrate," Science **306**, 469 (2004).
[13]T. A. Strobel, C. A. Koh, and E. Dendy Sloan, "Water cavities of sH clathrate hydrate stabilized by molecular hydrogen," J. Phys. Chem. B **112**, 1885 (2008).
[14]T. A. Strobel, E. Dendy Sloan, and C. A. Koh, "Raman spectroscopic studies of hydrogen clathrate hydrates," J. Chem. Phys. **130**, 014506 (2009).
[15]Z. Huo, K. Hester, E. Dendy Sloan, and K. T. Miller, "Methane hydrate nonstoichiometry and phase diagram," AIChE J. **49**, 1300 (2003).
[16]B. C. Barnes and A. K. Sum, "Advances in molecular simulations of clathrate hydrates," Curr. Opin. Chem. Eng. **2**, 184–190 (2013).
[17]H. Herzog, K. Caldeira, and E. Adams, "Carbon sequestration via direct injection," in *Encyclopedia of Ocean Sciences*, edited by J. Steele, S. Thorpe, and K. Turekian (Academic, London, 2001), Vol. 1, p. 408.
[18]P. Englezos, *Applications of Clathrate (Gas) Hydrates* (John Wiley & Sons, Ltd., 2022), Chap. 16, pp. 749–781.
[19]C. D. Ruppel and J. D. Kessler, "The interaction of climate change and methane hydrates," Rev. Geophys. **55**, 126–168, https://doi.org/10.1002/2016rg000534 (2017).
[20]H. Dashti, L. Zhehao Yew, and X. Lou, "Recent advances in gas hydrate-based $CO_2$ capture," J. Nat. Gas Sci. Eng. **23**, 195–207 (2015).
[21]B. R. Lee, C. A. Koh, and A. K. Sum, "Quantitative measurement and mechanisms for $CH_4$ production from hydrates with the injection of liquid $CO_2$," Chem. Chem. Phys. **16**, 14922–14927 (2014).
[22]T. Liu, P. Wu, Z. Chen, and Y. Li, "Review on carbon dioxide replacement of natural gas hydrate: Research progress and perspectives," Energy Fuels **36**, 7321–7336 (2022).
[23]A. Touil, D. Broseta, and A. Desmedt, "Gas hydrate crystallization in thin glass capillaries: Roles of supercooling and wettability," Langmuir **35**, 12569–12581 (2019).
[24]E. M. Freer, M. Sami Selim, and E. Dendy Sloan, Jr., "Methane hydrate film growth kinetics," Fluid Phase Equilib. **185**, 65–75 (2001).
[25]T. Uchida, T. Ebinuma, J. Kawabata, and H. Narita, "Microscopic observations of formation processes of clathrate-hydrate films at an interface between water and carbon dioxide," J. Cryst. Growth **204**, 348–356 (1999).
[26]J. D. Wells, W. Chen, R. L. Hartman, and C. A. Koh, "Carbon dioxide hydrate in a microfluidic device: Phase boundary and crystallization kinetics measurements with micro-Raman spectroscopy," J. Chem. Phys. **154**, 114710 (2021).
[27]H. D. Nagashima, M. Oshima, and Y. Jin, "Film-growth rates of methane hydrate on ice surfaces," J. Cryst. Growth **537**, 125595 (2020).
[28]W. Ou, W. Lu, K. Qu, L. Geng, and I.-M. Chou, "In situ Raman spectroscopic investigation of flux-controlled crystal growth under high pressure: A case study of carbon dioxide hydrate growth in aqueous solution," Int. J. Heat Mass Transfer **101**, 834–843 (2016).
[29]D. Daniel-David, F. Guerton, C. Dicharry, J.-P. Torré, and D. Broseta, "Hydrate growth at the interface between water and pure or mixed $CO_2$/$CH_4$ gases: Influence of pressure, temperature, gas composition and water-soluble surfactants," Chem. Eng. Sci. **132**, 118–127 (2015).
[30]P. Warrier, M. N. Khan, V. Srivastava, C. M. Maupin, and C. A. Koh, "Overview: Nucleation of clathrate hydrates," J. Chem. Phys. **145**, 211705 (2016).
[31]H. Bian, L. Ai, J. Y. Y. Heng, G. C. Maitland, and K. Hellgardt, "Effects of chemical potential differences on methane hydrate formation kinetics," Chem. Eng. J. **452**, 139084 (2023).
[32]H. Nada, "Growth mechanism of a gas clathrate hydrate from a dilute aqueous gas solution: A molecular dynamics simulation of a three-phase system," J. Phys. Chem. B **110**, 16526–16534 (2006).
[33]J. Grabowska, S. Blazquez, E. Sanz, E. G. Noya, I. M. Zeron, J. Algaba, J. M. Miguez, F. J. Blas, and C. Vega, "Homogeneous nucleation rate of methane hydrate formation under experimental conditions from seeding simulations," J. Chem. Phys. **158**, 114505 (2023).
[34]Arjun, T. A. Berendsen, and P. G. Bolhuis, "Unbiased atomistic insight in the competing nucleation mechanisms of methane hydrates," Proc. Natl. Acad. Sci. U. S. A. **116**, 19305–19310 (2019).
[35]S. A. Bagherzadeh, S. Alavi, J. Ripmeester, and P. Englezos, "Formation of methane nano-bubbles during hydrate decomposition and their effect on hydrate growth," J. Chem. Phys. **142**, 214701 (2015).
[36]A. H. Nguyen and V. Molinero, "Cross-nucleation between clathrate hydrate polymorphs: Assessing the role of stability, growth rate, and structure matching," J. Chem. Phys. **140**, 084506 (2014).
[37]B. C. Knott, V. Molinero, M. F. Doherty, and B. Peters, "Homogeneous nucleation of methane hydrates: Unrealistic under realistic conditions," J. Am. Chem. Soc. **134**, 19544–19547 (2012).
[38]M. R. Walsh, C. A. Koh, E. D. Sloan, A. K. Sum, and D. T. Wu, "Microsecond simulations of spontaneous methane hydrate nucleation and growth," Science **326**, 1095–1098 (2009).
[39]Y. Chen, C. Chen, and A. K. Sum, "Molecular resolution into the nucleation and crystal growth of clathrate hydrates formed from methane and propane mixtures," Cryst. Growth Des. **21**, 960–973 (2021).
[40]M. R. Walsh, G. T. Beckham, C. A. Koh, E. D. Sloan, D. T. Wu, and A. K. Sum, "Methane hydrate nucleation rates from molecular dynamics simulations: Effects of aqueous methane concentration, interfacial curvature, and system size," J. Phys. Chem. C **115**, 21241–21248 (2011).
[41]S. Sarupria and P. G. Debenedetti, "Homogeneous nucleation of methane hydrate in microsecond molecular dynamics simulations," J. Phys. Chem. Lett. **3**, 2942–2947 (2012).
[42]A. Arjun and P. G. Bolhuis, "Homogeneous nucleation of crystalline methane hydrate in molecular dynamics transition paths sampled under realistic conditions," J. Chem. Phys. **158**, 044504 (2023).
[43]A. M. Fernandez-Fernandez, M. M. Conde, G. Perez-Sanchez, M. Pérez-Rodríguez, and M. M. Pineiro, "Molecular simulation of methane hydrate growth confined into a silica pore," J. Mol. Liq. **362**, 119698 (2022).
[44]J. R. Espinosa, C. Navarro, E. Sanz, C. Valeriani, and C. Vega, "On the time required to freeze water," J. Chem. Phys. **145**, 211922 (2016).
[45]P. Montero de Hijes, J. Espinosa, C. Vega, and E. Sanz, "Ice growth rate: Temperature dependence and effect of heat dissipation," J. Chem. Phys. **151**, 044509 (2019).
[46]M. M. Conde and C. Vega, "Determining the three-phase coexistence line in methane hydrates using computer simulations," J. Chem. Phys. **133**, 064507 (2010).
[47]J. M. Miguez, M. M. Conde, J. P. Torre, F. J. Blas, M. M. Pineiro, and C. Vega, "Molecular dynamics simulation of $CO_2$ hydrates: Prediction of three phase coexistence line," J. Chem. Phys. **142**, 124505 (2015).

[48]S.-L. Li, C.-Y. Sun, B. Liu, Z.-Y. Li, G.-J. Chen, and A. K. Sum, "New observations and insights into the morphology and growth kinetics of hydrate films," Sci. Rep. **4**, 4129 (2014).
[49]Y.-T. Tung, L.-J. Chen, Y.-P. Chen, and S.-T. Lin, "The growth of structure I methane hydrate from molecular dynamics simulations," J. Phys. Chem. B **114**, 10804–10813 (2010).
[50]J. L. F. Abascal, E. Sanz, R. García Fernández, and C. Vega, "A potential model for the study of ices and amorphous water: TIP4P/Ice," J. Chem. Phys. **122**, 234511 (2005).
[51]B. Guillot and Y. Guissani, "A computer simulation study of the temperature dependence of the hydrophobic hydration," J. Chem. Phys. **99**, 8075–8094 (1993).
[52]D. Paschek, "Temperature dependence of the hydrophobic hydration and interaction of simple solutes: An examination of five popular water models," J. Chem. Phys. **120**, 6674–6690 (2004).
[53]J. J. Potoff and J. I. Siepmann, "Vapor–liquid equilibria of mixtures containing alkanes, carbon dioxide, and nitrogen," AIChE J. **47**, 1676–1682 (2001).
[54]D. van der Spoel, E. Lindahl, B. Hess, G. Groenhof, A. E. Mark, and H. J. C. Berendsen, "GROMACS: Fast, flexible, and free," J. Comput. Chem. **26**, 1701 (2005).
[55]B. Hess, C. Kutzner, D. van der Spoel, and E. Lindahl, "GROMACS 4: Algorithms for highly efficient, load-balanced, and scalable molecular simulation," J. Chem. Theory Comput. **4**, 435–447 (2008).
[56]D. Beeman, "Some multistep methods for use in molecular dynamics calculations," J. Comput. Phys. **20**, 130–139 (1976).
[57]S. Nosé, "A molecular dynamics method for simulations in the canonical ensemble," Mol. Phys. **52**, 255–268 (1984).
[58]W. G. Hoover, "Canonical dynamics: Equilibrium phase-space distributions," Phys. Rev. A **31**, 1695–1697 (1985).
[59]M. Parrinello and A. Rahman, "Polymorphic transitions in single crystals: A new molecular dynamics method," J. Appl. Phys. **52**, 7182–7190 (1981).
[60]U. Essmann, L. Perera, M. L. Berkowitz, T. Darden, H. Lee, and L. G. Pedersen, "A smooth particle mesh Ewald method," J. Chem. Phys. **103**, 8577–8593 (1995).
[61]B. Hess, H. Bekker, H. J. C. Berendsen, and J. G. E. M. Fraaije, "LINCS: A linear constraint solver for molecular simulations," J. Comput. Chem. **18**, 1463 (1997).
[62]B. Hess, "P-LINCS: A parallel linear constraint solver for molecular simulation," J. Chem. Theory Comput. **4**, 116–122 (2008).
[63]J. R. Espinosa, J. L. F. Abascal, L. F. Sedano, E. Sanz, and C. Vega, "On the possible locus of the liquid–liquid critical point in real water from studies of supercooled water using the TIP4P/Ice model," J. Chem. Phys. **158**, 204505 (2023).
[64]D. Turnbull, "Under what conditions can a glass be formed?," Contemp. Phys. **10**, 473–488 (1969).
[65]H. R. Pruppacher, "Interpretation of experimentally determined growth rates of ice crystals in supercooled water," J. Chem. Phys. **47**, 1807–1813 (1967).
[66]J. Algaba, I. Zeron, J. M. Miguez, J. Grabowska, S. Blazquez, E. Sanz, C. Vega, and F. Blas, "Solubility of carbon dioxide in water: Some useful results for hydrate nucleation," J. Chem. Phys. **158**, 184703 (2023).
[67]J. Grabowska, S. Blazquez, E. Sanz, I. M. Zerón, J. Algaba, J. M. Míguez, F. J. Blas, and C. Vega, "Solubility of methane in water: Some useful results for hydrate nucleation," J. Phys. Chem. B **126**, 8553–8570 (2022).
[68]S. Blazquez and C. Vega, "Melting points of water models: Current situation," J. Chem. Phys. **156**, 216101 (2022).
[69]A. M. Fernández-Fernández, M. Pérez-Rodríguez, A. Comesana, and M. M. Pineiro, "Three-phase equilibrium curve shift for methane hydrate in oceanic conditions calculated from molecular dynamics simulations," J. Mol. Liq. **274**, 426 (2019).
[70]S. Blazquez, C. Vega, and M. M. Conde, "Three phase equilibria of the methane hydrate in NaCl solutions: A simulation study," J. Mol. Liq. **383**, 122031 (2023).
[71]M. M. Conde, M. Rovere, and P. Gallo, "High precision determination of the melting points of water TIP4P/2005 and water TIP4P/Ice models by the direct coexistence technique," J. Chem. Phys. **147**, 244506 (2017).
[72]M. M. Conde and C. Vega, "Note: A simple correlation to locate the three phase coexistence line in methane-hydrate simulations," J. Chem. Phys. **138**, 056101 (2013).
[73]D. Rozmanov and P. G. Kusalik, "Temperature dependence of crystal growth of hexagonal ice ($I_h$)," Phys. Chem. Chem. Phys. **13**, 15501–15511 (2011).
[74]D. Rozmanov and P. G. Kusalik, "Anisotropy in the crystal growth of hexagonal ice, $I_h$," J. Chem. Phys. **137**, 094702 (2012).
[75]M. A. Carignano, P. B. Shepson, and I. Szleifer, "Molecular dynamics simulations of ice growth from supercooled water," Mol. Phys. **103**, 2957–2967 (2005).